Bioactive Materials 44 (2025) 474–487

Contents lists available at ScienceDirect

Bioactive Materials

journal homepage: www.keaipublishing.com/en/journals/bioactive-materials

Nanoclay gels attenuate BMP2-associated inflammation and promote chondrogenesis to enhance BMP2-spinal fusion

Takuya Furuichi [a], Hiromasa Hirai [a], Takayuki Kitahara [a], Masayuki Bun [a], Masato Ikuta [a], Yuichiro Ukon [a], Masayuki Furuya [a], Richard O.C. Oreffo [b], Agnieszka A. Janeczek [c], Jonathan I. Dawson [b], Seiji Okada [a], Takashi Kaito [a,*]

[a] Department of Orthopedic Surgery, Osaka University Graduate School of Medicine, 2-2 Yamadaoka, Suita, Osaka, 565-0871, Japan
[b] Bone & Joint Research Group, Centre for Human Development, Stem Cells & Regeneration, Institute of Developmental Sciences, University of Southampton, Southampton, SO16 6YD, United Kingdom
[c] Renovos Biologics Limited, 2 Venture Road, University of Southampton Science Park, Southampton, SO16 7NP, United Kingdom

ARTICLE INFO

Keywords:
Nanoclay
Bone morphogenetic protein 2
Endochondral ossification
Inflammation
Bone tissue engineering

ABSTRACT

Bone morphogenetic protein 2 (BMP2) is clinically applied for treating intractable fractures and promoting spinal fusion because of its osteogenic potency. However, adverse effects following the release of supraphysiological doses of BMP2 from collagen carriers are widely reported. Nanoclay gel (NC) is attracting attention as a biomaterial, given the potential for localized efficacy of administered agents. However, the efficacy and mechanism of action of NC/BMP2 remain unclear. This study explored the efficacy of NC as a BMP2 carrier in bone regeneration and the enhancement mechanism. Subfascial implantation of NC containing BMP2 elicited superior bone formation compared with collagen sponge (CS). Cartilage was uniformly formed inside the NC, whereas CS formed cartilage only on the perimeter. Additionally, CS induced a dose-dependent inflammatory response around the implantation site, whereas NC induced a minor response, and inflammatory cells were observed inside the NC. In a rat spinal fusion model, NC promoted high-quality bony fusion compared to CS. *In vitro,* NC enhanced chondrogenic and osteogenic differentiation of hBMSCs and ATDC5 cells while inhibiting osteoclastogenesis. Overall, NC/BMP2 facilitates spatially controlled, high-quality endochondral bone formation without BMP2-induced inflammation and promotes high-density new bone, functioning as a next-generation BMP2 carrier.

1. Introduction

Critical-sized bone defects from trauma, tumor resection, non-union fractures, or spinal fusion surgery rarely heal spontaneously. Autogenous bone grafting remains the gold standard treatment despite limitations in donor site morbidity, available bone quantity, and age-related deterioration in harvested bone quality [1–4]. Additionally, artificial bones and allografts lack biological activity, functioning only as bone graft extenders, which limits their potential for bone formation. Meanwhile, bone morphogenetic protein 2 (BMP2) can independently replicate all processes necessary for osteogenesis, including inflammatory responses, mesenchymal stem cell migration, and endochondral ossification. Therefore, BMP2 is expected to serve as a bone graft material alternative to autografts.

BMPs, members of the transforming growth factor (TGF)-β superfamily, were discovered over six decades ago in the seminal studies of Marshall Urist to hold potent osteoinductive capacity [5–7]. Clinically, BMP has been combined with collagen carriers to form biological bone grafting materials in the United States and Europe since the early 2000s [8,9]. However, in addition to its less-than-expected effects in promoting bone fusion, complications related to inflammatory reactions due to the rapid release of non-physiologically high doses of BMP from the

Abbreviations: NC, nanoclay gel; ROIs, regions of interest; GM, growth medium; ODM, osteogenic differentiation medium; CST, Cell Signaling Technology; MNGCs, multinucleated giant cells; CS, collagen sponge; IVIS, *in vivo* imaging system; sGAG, sulfated glycosaminoglycan; BMDM, bone marrow-derived macrophages.

Peer review under responsibility of KeAi Communications Co., Ltd.

* Corresponding author.
E-mail address: takashikaito@ort.med.osaka-u.ac.jp (T. Kaito).

https://doi.org/10.1016/j.bioactmat.2024.10.027
Received 18 May 2024; Received in revised form 30 October 2024; Accepted 30 October 2024
Available online 5 November 2024

collagen carriers into surrounding tissues have hampered widespread clinical application. Only micrograms of BMPs per kilogram are present in the demineralized bone matrix, whereas milligrams of BMPs are used in clinical practice [10]. BMP2 use at a supraphysiological dose in humans is associated with myriad widely reported side effects, such as inflammation, osteolysis, edema, inappropriate adipogenesis, and ectopic bone formation [11–17]. Thus, it is critical to identify carriers that can harness and localize the osteogenic potential of BMPs without inducing inflammatory reactions at the bone site.

Nanoclays, also known as synthetic hectorites, are lithium magnesium sodium silicates composed of disc-shaped particles formed by a central magnesium sheet surrounded by two silica sheets. Due to lithium substitutions in the magnesium sheet, nanoclay particles possess a permanent negative surface charge and a positive charge at the particle edges at neutral pH. When dispersed in water, nanoclay particles disperse and self-assemble into thixotropic gels, which can encapsulate and localize bioactive molecules *via* electrolyte-induced gelation and protein-clay electrostatic interactions [18]. Nanoclays biodegrade into biocompatible ions (Mg, Li, Si) released through intracellular degradation pathways. They also enhance the osteogenic differentiation of human mesenchymal stromal cells *in vitro* [19–22].

The following structural and compositional features contribute to the long-term retention of BMP2 by nanoclay. The layered structure of nanoclay physically entraps BMP2. Additionally, the negatively charged surface of nanoclay interacts electrostatically with the positively charged BMP2 molecules, delaying their release [23,24]. The ability to localize and deliver bioactive factors using nanoclay suggests that it could offer an innovative BMP-delivery carrier material for bone regeneration. Accordingly, in the present study, we assessed the potential of RENOVITE®, a synthetic hectorite manufactured specifically for medical applications, *in vitro* and *in vivo,* to modulate bone formation. The results demonstrate that RENOVITE® potentiates BMP-induced new bone by enhancing endochondral bone formation in the absence of a dose-dependent inflammatory response.

2. Materials and methods

2.1. NC preparation

RENOVITE®, a synthetic hectorite (similar to LAPONITE®) manufactured by Renovos Biologics (Southampton, UK), is a lithium magnesium sodium silicate composed of particles measuring 25–30 nm in diameter and 1 nm thickness, with the chemical formula Na_8^+ $[(Si_8Mg_{5.9}Li_{0.4})O_{20}(OH)_4]$. A modified ratio of compositional ions in RENOVITE® improves the gelation reaction in serum and ensures high stability under physiological conditions for effective localized application at the implant site, enhancing handling for biomedical applications (U.S. Patent No. 12,036,328). RENOVITE® particles have a permanent negative surface charge and a positive edge charge. RENOVITE® nanoclay gel (NC) was prepared as described previously (Fig. S2a) [25]. In brief, RENOVITE® powder was dispersed in distilled water to obtain the required concentration % weight of NC per unit volume.

For *in vitro* studies, NC was adjusted to 5 mg/mL using sterile water and thoroughly agitated at 25 °C for 30 min. The NC solution was added to the culture medium at 0, 1, 10, 30, 50, or 100 μg/mL. For *in vivo* studies, NC was adjusted to 35 mg/mL using sterile water (3.5 % weight NC per unit volume). At this concentration, NC transitioned into a gel simply by dissolving in water. This transformation occurs because at concentrations >3 wt%, the particles densely arrange into a “house of cards” structure, ultimately forming nematic gels (liquid crystals) [24]. Furthermore, at concentrations of 3 %, NC exhibits minimal dispersion *in vitro* [26]. The NC preparations were sterilized by autoclaving, and the evaporated water was replenished. *Escherichia coli*-derived recombinant human BMP2 used in this study was kindly provided by CGBio (Seoul, Korea), and was adjusted to 1 μg/μL.

2.2. Evaluation of NC properties

The X-ray diffraction (XRD) analysis of RENOVITE® powder was conducted with a D2 Phaser X-ray diffractometer (Bruker, Billerica, MA, USA) using Cu Kα radiation (λ = 1.54184 Å, 30 kV, 0.2 Time/Step (s) and 10 mA). The diffraction pattern was recorded over a 2θ range of 20°–60° to confirm the phase and crystallinity of the material. Fourier-transform infrared (FTIR) spectroscopy was performed using a Nicolet iS5 FTIR spectrometer with an iD7 ATR accessory (Thermo Scientific, Waltham, MA, USA). The spectra were collected from 4000 to 400 cm^{-1} to identify the functional groups present in RENOVITE®. Transmission electron microscopy (TEM) was conducted to investigate the morphology of RENOVITE® particles. Suspensions of RENOVITE® (0.001 %) deposited and dried on a grid, as well as 2.8 % RENOVITE® NC dehydrated and embedded in resin were imaged using a HT770 transmission electron microscopy (Hitachi High-Tech, Tokyo, Japan).

2.3. Evaluation of gelation

To assess the differences in gelation when exposed to serum, 40 μL of 3.5 % RENOVITE® NC was placed on a coverslip and positioned at the bottom of a 6-cm dish. The dish was filled with distilled water or fetal bovine serum (FBS; Equitech-Bio, Kerrville, TX, USA). After 5 min, photographs of the NC appearance were captured. Rheometric evaluations were conducted to investigate the gelation exposed to serum. Rheological measurements were performed using a 25 mm parallel-plate HAAKE™ MARS™ rheometer (Thermo Scientific). A 1.5 mL volume of 3.5 % RENOVITE® NC or LAPONITE XLG® (synthetic hectorite clay produced by BYK Additives, Widnes, UK) NC was applied to the rheometer plate, maintained at 25 °C with a 2.5 mm gap. Initial measurements of the storage modulus (G′) and loss modulus (G″) were recorded for 2 min at a constant oscillatory strain of 0.1 % and an angular frequency of 1 rad/s. PBS (pH 7.4) or serum (40 mg/mL bovine serum albumin in PBS, pH 7.4) was then introduced to the level of the underside of the upper plate. Subsequent storage and loss modulus changes over time due to exposure to PBS or serum were recorded.

2.4. Mouse subfascial implantation model

We developed a mouse subfascial implantation model to mimic the bone formation process triggered by BMP2. This model is recognized for its high reproducibility in inducing ectopic bone formation by BMP2 [27] and is well-suited for quantitative evaluation of the effects and potential side effects of BMP2 [28]. An absorbable collagen sponge (CS) (CollaCote; Zimmer Dental, Carlsbad, CA, USA) was cut into circular discs (5 mm in diameter and 2 mm thick) and soaked with 1, 5, or 10 μg of BMP2 dissolved in 10 μL of sterile PBS. Forty microliters of 3.5 % NC were prepared and mixed by vigorous vortexing in collection tubes with 1, 5, or 10 μg BMP2 dissolved in 10 μL of sterile PBS. CS and NC, mixed with the same volume of PBS without BMP2, were prepared as controls. Eight-week-old C57BL/6J male mice were purchased from Jackson Laboratory Japan (Kanagawa, Japan). CS and NC were implanted under the left and right fascia of the gluteus maximus muscle. The gluteus maximus fascia was exposed, and pockets were created under the fascia. A CS disc and NC were then implanted in the respective pockets [29]. On days 7, 10, 14, and 21 post-surgery, histological assessment of cartilage formation was performed. Bone formation was evaluated by micro-CT and histological analysis. The overview of this experiment is presented in Fig. 1. All animal experiments were approved by the Animal Experimental Committee of Osaka University Graduate School of Medicine and restrictedly followed ARRIVE guidelines and the National Institutes of Health Guide for the Care and Use of Laboratory Animals.

2.5. Assessment of BMP2 localization capacity of NC

BMP2 was fluorescently labeled using an amine-reactive (NHS ester)

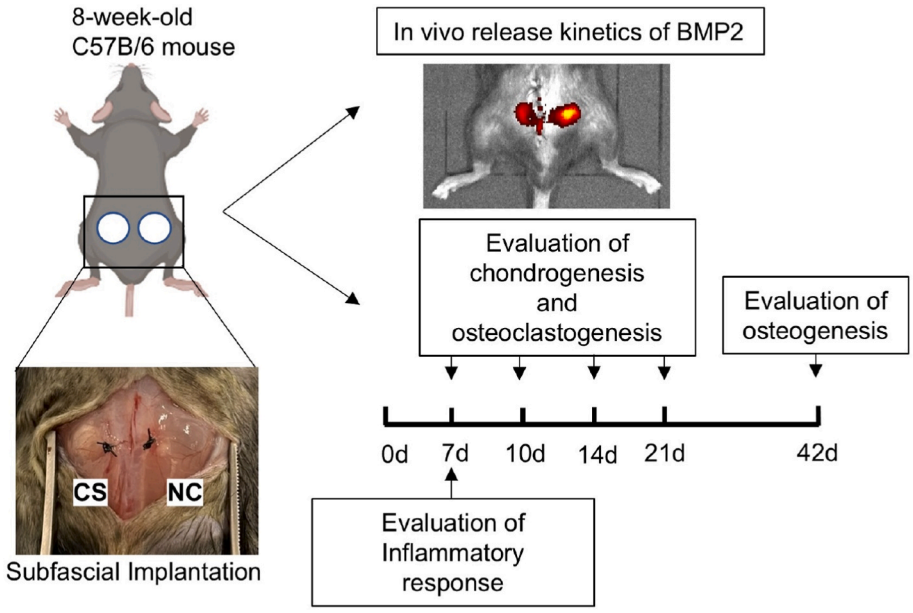

Fig. 1. Overview of the subfascial implantation mouse model. Following implantation of test materials beneath the fascia, the following evaluations were performed at the indicated time points: release kinetics of BMP2 and inflammatory response (on day 7), chondrogenesis (on days 7, 10, 14, and 21), osteoclastogenesis (on days 7, 10, 14, 21 and 42), and osteogenesis (on day 42).

near-infrared fluorochrome (VivoTag-S750), as described in a previous report [30]. Fluorescence imaging was performed using an IVIS. For *in vitro* localization tests, CS discs and 40 μL of 3.5 % NC mixed with 0.1, 0.5, or 1 μg of labeled BMP2 dissolved in 10 μL of sterilized PBS were placed at the bottom of 24-well plate wells filled with 1 mL of PBS. The PBS was replaced after each measurement. The total fluorescence count and radiance efficiency were assessed at 0, 3, 6, 12, and 24 h, and daily thereafter up to 7 days. For *in vivo* localization tests, CS discs and 40 μL of 3.5 % NC mixed with 1 and 2 μg of labeled BMP2 dissolved in 10 μL of sterilized PBS were implanted under the fascia of the gluteus maximus muscle of 8-week-old C57BL/6J male mice. The total fluorescence count and radiance efficiency were assessed at 0, 3, 6, 12, and 24 h, and daily thereafter up to 7 days. Fluorescence signals were normalized to the signal at the 0-h time point, and exponential decay curves were created. Imaging data were analyzed using IVIS Living Image Software (version 4.0; Caliper Life Sciences, Waltham, MA, USA).

2.6. Evaluation of ectopic bone formation in mouse subfascial implantation model

2.6.1. Micro-CT analysis

On days 21 and 42 after subfascial implantation, CS and NC containing 0 or 1 μg of BMP2 diluted in 10 μL of PBS were harvested and scanned using *ex vivo* high-resolution micro-CT (SkyScan 1272; Bruker) with a 80 kV source voltage, 125 μA source current, and 15 μm pixel size. Analysis was performed using CTAN software (version 1.18.8.0, Brucker).

2.6.2. Histological analysis

On days 7, 10, 14, 21, and 42, CS and NC containing 1 μg of BMP2 were explanted, fixed with 10 % formalin, decalcified with 10 % ethylenediaminetetraacetic acid, dehydrated in an ethanol series, embedded in paraffin wax, serially sectioned at 3.5 μm thickness, and stained with hematoxylin and eosin (H&E), safranin-O (both from Muto Pure Chemicals, Tokyo, Japan), and tartrate-resistant acid phosphatase (TRAP) (Cosmo Bio, Tokyo, Japan) according to the manufacturer's protocol. Osteoclasts were quantified by counting the TRAP-stained cells in the carrier per section and dividing the cell number by the area of the carrier per section.

2.6.3. Quantification of sulfated glycosaminoglycans

Implanted CS and NC were explanted on days 7, 10, 14, and 21 and digested with 0.05 % papain (Sigma–Aldrich, St. Louis, MO, USA) at 65 °C for 18 h. Sulfated glycosaminoglycan (sGAG) was quantified using a dimethyl methylene blue dye-binding assay (Blyscan Glycosaminoglycan Assay Kit; Biocolor, Westbury, NY, USA).

2.7. Evaluation of the inflammatory response in the mouse subfascial implantation model

To evaluate the inflammatory response induced by BMP2, CS discs (5 mm diameter, 2 mm height) and NC (40 μL) containing 0, 1, 5, or 10 μg of BMP2 dissolved in 10 μL of sterilized PBS were implanted under the right and left gluteus maximus fascia of 8-week-old mice. In clinical practice, inflammatory reactions such as hematoma and swelling typically occur during the first postoperative week [31,32]. Therefore, inflammatory reactions were evaluated on postoperative day 7. The implanted CS and NC were harvested on day 7 and subjected to H&E and immunohistochemical staining. Antibodies targeting CD68 (ab125212; Abcam, Cambridge, UK), neutrophils (ab53457; Abcam), CD206 (24595; CST, Danvers, MA, USA), TNF-α (GTX110520; GeneTex, Irvine, CA, USA), and SOX9 (ab185230; Abcam) were visualized using Histofine Simple Stain MAX PO and Simple Stain DAB Solution (both from Nichirei Bioscience, Tokyo, Japan). Inflammatory areas characterized by inflammatory cell infiltration were quantified using ImageJ software (version 1.53t; National Institutes of Health, Bethesda, MD, USA). The numbers of CD68-positive cells, neutrophils, TRAP-positive cells, CD206-positive multinucleated giant cells (MNGCs), and TNF-α-positive cells were counted in the inflammatory cell infiltrate layer (300 × 300 μm, two fields/sample for CD68, neutrophils, TRAP, and CD206, one field/sample for TNF-α) as previously described [33]. To evaluate the localization of undifferentiated (SOX9-positive) cells in the inflammatory cell infiltrate around carriers containing 5 μg BMP2, four arbitrary 300 × 600 μm rectangular regions of interest (ROIs) were defined around the boundary between the carrier and the tissue, and SOX9-positive cells were quantified inside and outside the boundary.

2.8. Rat spinal fusion model

For spinal posterolateral fixation, 32 eight-week-old male Sprague–Dawley rats (The Jackson Laboratory Japan) were divided into four groups based on the carrier material (CS or NC) and BMP2 dose (5 μg or 10 μg; Table S1). On postoperative day 42, the rats were euthanized with an overdose of isoflurane (Viatris, Tokyo, Japan), and the treated spinal segments were harvested.

2.8.1. Surgical procedure

A longitudinal incision was made along the posterior midline of the skin. Additionally, two incisions were made paramedial in the lumbar fascia, positioned 2 mm away from the midline. After exposing the transverse processes of the L4 and L5 vertebrae, they were decorticated with a high-speed burr until blood oozed from the bone marrow. Then, 5 or 10 μg of BMP2 dissolved in 20 μL of sterilized PBS was applied to 5 × 10 × 1 mm^3 CS and 50 μL of 3.5 % NC before implantation on the posterior transverse processes.

2.8.2. Micro-CT analysis of treated spine

Extracted spinal segments were scanned using high-resolution micro-CT (SkyScan 1272) with the following parameters: source voltage = 80 kV, source current = 125 μA, image pixel size = 13.3 μm, rotation step = 1, and filter = Al 1 mm. Spinal fusion was defined by bridging new bone formation between the L4 and L5 transverse processes. To analyze the bone quality of the newly formed fusion mass, a 1.5 × 3 × 1 mm^3 cuboid ROI was set at the center of the fusion mass. In anterior forehead sections, a rectangular ROI composed of a line passed through the L4/5 disc space and the center of the transverse process, each 1.5 mm cephalad and caudal, 1.5 mm wide; in transverse sections, it passed 1 mm anterior to the line of the posterior margin of the vertebral body (Fig. 6B). Image analysis was performed using CTAN software (version 1.18.8.0, Brucker).

2.8.3. Histological analysis of treated spine

Explanted spinal segments fixed in 10 % formalin were demineralized using KCX solution (Falma, Tokyo, Japan), dehydrated in ethanol, and embedded in paraffin wax. Coronal sections of 5 μm thickness were cut at the level of the anterior 1/3 of the vertebral body. Newly formed trabecular bone inside the fusion mass between the L4 and L5 transverse processes was quantified using H&E staining. A 1.5 × 3 mm^2 ROI was set inside the fusion mass centered at the L4/5 disc level, craniocaudal within the spinal fusion area, centered at the L4/5 disc level. Trabecular bone and adipose tissue area within the ROI were color-coded and quantified using ImageJ (version 1.53t).

2.9. In vitro osteogenic differentiation assay

Mouse-derived MC3T3-E1 preosteoblasts (Riken Cell Bank, Tsukuba, Japan) and human bone marrow stromal cells (hBMSCs; Lonza, Cologne, Germany) were seeded in 24-well culture plates at a density of 5.0 × 10^4 cells/well at passage 6. The cells were cultured in a growth medium (GM) comprising α-minimum essential medium (α-MEM) supplemented with 10 % FBS and 1 % penicillin and streptomycin (Sigma–Aldrich, St. Louis, MO, USA). When the cells reached confluence, the GM was replaced with osteogenic differentiation medium (ODM), comprising GM supplemented with 50 μg/mL L-ascorbic acid 2-phosphate (Sigma–Aldrich), 10 mM β-glycerol phosphate (Merck KGaA, Frankfurt, Germany), and 10 nM dexamethasone (Sigma–Aldrich). NC was dissolved in ODM at 1, 10, 30, and 50 μg/mL for MC3T3-E1 and at 1, 10, and 100 μg/mL for hBMSCs. qPCR analysis was performed on day 3 for hBMSCs and day 7 for MC3T3-E1. ALP staining and ALP activity were evaluated on day 7 for MC3T3-E1 and hBMSCs, and Alizarin red staining was performed on day 21 for hBMSCs.

2.9.1. ALP staining and activity

After culturing MC3T3-E1 cells and hBMSCs for 7 days, the cells were washed twice with PBS, and attached cells were fixed using 500 μL of 4 % paraformaldehyde for 30 min. After two rinses with distilled water, BCIP/NBT Color Development Substrate (Promega, Madison, WI, USA) was used for ALP staining. To assess ALP activity, 100 μL of M-PER was added to each well, and the cells were detached using mini scrapers. The supernatant was collected for ALP assays using the Lab Assay ALP kit (Wako Pure Chemical Industries, Osaka, Japan).

2.9.2. Alizarin red staining

After culturing hBMSCs in ODM for 21 days, the cells were washed twice with PBS, and the attached cells were fixed in 4 % paraformaldehyde. After two rinses with distilled water, the cells were stained with 500 μL of Alizarin Red solution (Muto Pure Chemicals) at room temperature for 30 min. The dye was extracted with 5 % formic acid, and the absorbance at 405 nm was determined using a Multiskan GO instrument and SkanIt software (Thermo Scientific).

2.10. In vitro chondrogenic differentiation assay

Mouse-derived teratocarcinoma cells (ATDC5; Riken Cell Bank) were cultured and maintained in Dulbecco's modified Eagle's medium (DMEM)/F-12 medium supplemented with 5 % FBS and 1 % antibiotic-antimitotic. To induce chondrogenic differentiation, ATDC5 cells were seeded in 24-well culture plates at a density of 5.0 × 10^4 cells/well at passage 8, along with 1 % ITS + Premix Universal Supplement (Corning, New York, NY, USA), and NC was added at 1, 10, or 100 μg/mL. The hBMSCs were cultured in chondrogenic medium comprising DMEM containing 1 % ITS + Premix Universal Supplement (Corning), 50 μg/mL ascorbic acid (Sigma–Aldrich), 40 μg/mL L-proline (Wako), 100 nM dexamethasone (Sigma–Aldrich), 10 ng/mL transforming growth factor β3 (PeproTech, Rocky Hill, NJ, USA), and 1 % antibiotic-antimitotic. The hBMSCs were suspended at a concentration of 1 × 10^7 cells/mL. Subsequently, 10-μL droplets of the cell suspension were gently deposited into the interior of each well in a 24-well plate and allowed to adhere at 37 °C for 2 h. Then, 500 μL of chondrogenic medium containing 1, 10, or 100 μg/mL NC was introduced to each well. ATDC5 cells were assessed by qPCR and Alcian blue staining on day 7, whereas hBMSCs were evaluated by Alcian blue staining on day 21.

2.10.1. Alcian blue staining

After washing with PBS, the cells were fixed in 500 μL of 4 % paraformaldehyde for 10 min, followed by two washes with distilled water. Then, they were incubated with 1 % acetic acid for 5 min, succeeded by an overnight incubation at 25 °C in 500 μL of Alcian blue solution (pH 1.0; Muto Pure Chemicals). After adequate rinsing with distilled water, the dye was eluted using 6M guanidine hydrochloride and the absorbance at 595 nm was measured. ImageJ (version 1.53t) was used to quantify the area of Alcian blue-stained hBMSCs.

2.11. In vitro osteoclast differentiation assay

Murine primary osteoclasts were obtained from bone marrow cells flushed from the femurs and tibiae of C57BL/6J mice. The cells were cultured in α-minimum essential medium (MEM) containing 10 % FBS, 1 % penicillin and streptomycin, and 25 ng/mL macrophage colony-stimulating factor (M-CSF; R&D Systems, Minneapolis, MN, USA) at 37 °C overnight. Non-adherent cells were washed twice with PBS, and adherent cells were seeded in 24-well plates at 1 × 10^5 cells/well and cultured in 25 ng/mL M-CSF for three days to differentiate into bone marrow-derived macrophages (BMDMs). The cells were stimulated with 25 ng/mL M-CSF and 50 ng/mL receptor activator of nuclear factor kappa B ligand (RANKL; R&D Systems), and 200 ng/mL BMP2 was administered. On day 3, after RANKL administration, the medium was replaced with fresh medium, and on day 6, TRAP staining (Cosmo Bio)

and qPCR analysis were performed.

2.12. Cytotoxicity test

The cytotoxicity of NC dissolved in the culture medium was evaluated using the WST-8 assay (Nacalai Tesque, Kyoto, Japan). MC3T3-E1 cells, ATDC5 cells, hBMSCs, and BMDMs were seeded in 96-well tissue culture plates (5.0×10^3 cells/well). After 24 h, the medium was replaced with one containing NC. The plates were then further cultured for 1, 2, 3, 5, and 7 days, and cell proliferation was assessed according to the manufacturer's protocol.

2.13. In vitro co-culture experiments

MC3T3-E1 cells were seeded in 24-well tissue culture plates (5.0×10^4 cells/well). After reaching 100 % confluence, culture insert chambers (Falcon Cell Culture Inserts; pore size = 0.4 μm) containing CS or NC with or without 500 ng of BMP2 were suspended above each well. A vacant chamber (chamber only) group was used as a control, and the chamber containing PBS with 500 ng of BMP2 was used as a positive control. The medium was changed after 4 days of co-culture. ALP staining and activity were assessed after 3 and 7 days of co-culture.

2.14. qPCR

Total RNA was extracted using a RNeasy kit (Qiagen, Hilden, Germany) and reverse-transcribed into cDNA using ReverTra Ace qPCR RT Master Mix (Toyobo, Osaka, Japan). qPCR assays were run using SYBR Green Master Mix in a StepOnePlus Real-Time PCR System. Target gene expression levels were normalized to *GAPDH*, and fold changes were calculated relative to the control group using the $2^{-\Delta\Delta Ct}$ method [34]. Primers used in this study are presented in Table S2.

2.15. Western blotting

ATDC5 cells were plated in 6-well plates (3.0×10^5 cells/well) with DMEM/F-12 medium containing 5 % FBS and 1 % antibiotics. When the cells reached 100 % confluence, the medium was replaced with medium containing 1, 10, or 100 μg/mL NC, and the cells were incubated for 16 h. Cellular proteins were extracted using RIPA buffer (Nacalai Tesque) supplemented with a 1 % protease/phosphatase inhibitor cocktail (CST). For each sample, 25 μg of protein was subjected to sodium dodecyl sulfate-polyacrylamide gel electrophoresis (Thermo Scientific), followed by transfer to polyvinylidene difluoride membranes (Nippon Genetics, Tokyo, Japan). The membranes were blocked with 5 % skim milk in Tris-buffered saline Tween-20 at 25 °C for 1 h. Subsequently, they were probed with primary antibodies against phospho-SMAD1/5 (5753, 1:1000; CST), total SMAD1 (9743, 1:1000; CST), phospho-p44/42 MAPK (ERK1/2) (9101, 1:1000; CST), phospho-p38 MAPK (9211, 1:1000; CST), and β-actin (4970, 1:1000, CST) at 4 °C overnight, followed by incubation with a horseradish peroxidase-conjugated secondary antibody (7074, 1:1000; CST) for 1 h. Immunoreactivity was visualized using Amersham ECL Select Western Blotting Reagent (Cytiva, Tokyo, Japan) and a ChemiDoc MP Imaging System (Bio-Rad, Hercules, CA, USA).

2.16. Statistical analysis

Data were presented as mean ± standard deviation (SD). The means of two groups were compared using the unpaired Student's *t*-test, whereas one-way analysis of variance (ANOVA), followed by Dunnett multiple comparison tests or two-way ANOVA, followed by Bonferroni tests, were used to compare means of three or more groups. Statistical analysis was conducted using GraphPad Prism 9.4.1. Statistical significance was set at $p < 0.05$.

3. Results

3.1. Characterization of NC properties

The XRD diffractogram obtained for RENOVITE® confirmed a typical Na-synthetic hectorite without phase transformation or precipitate impurities (hk0, 0k0, 00l and h00 reflections in the low angle region (2θ = 20–40°), with d110, 020 = 4.5 A° at 2θ–20°, d004 = 3.18 A° at 2θ–28°, and d130, 200 = 2.56 A° at 2θ–35°; and hk0 and 0k0 reflections in the high angle region (2θ = 50–61°), with d150, 240, 310 = 1.72 A° at 2θ–53° and d060, 330 = 1.52 A° at 2θ–61°) (Fig. S1a). FTIR revealed stretching/bending vibrations of the functional group's characteristic of magnesium silicate clay mineral, including i) Si–O starching and Si–O–Si bending of the tetrahedral sheet (980, 427 cm^{-1}), ii) Mg–OH bending of the octahedral sheet (650 cm^{-1}), iii) H–O–H bending of adsorbed water, and iv) H–O stretching of interlayer water (Fig. S1b). TEM of a suspension of RENOVITE® particles (0.001 wt %) dried onto a surface revealed a round disk-shaped surface profile for 15–30 nm particles (Fig. S1c top). Meanwhile, TEM of an arrested RENOVITE® NC (2.8 wt %) dehydrated and embedded in resin revealed delamination of the RENOVITE® particles (Fig. S1c bottom).

RENOVITE® NC (the NC used in this study) exhibited an enhanced gelation reaction compared with LAPONITE® NC. In fact, RENOVITE® NC achieved a strength sufficient to be grasped with forceps when exposed to FBS (Fig. S2c). In addition, we conducted a rheological analysis of the physical properties of RENOVITE® NC and LAPONITE® NC after exposure to PBS or serum at physiological pH, simulating *in vivo* implantation conditions. In its native state, the G′ and G″ of RENOVITE® NC were comparable to those of LAPONITE® NC. However, the increases in G′ and G″ after exposure to PBS or serum were significantly greater for RENOVITE® than LAPONITE® (Figs. S2d and e). Upon exposure to PBS or serum, LAPONITE® NC showed a 3.5-fold and 8.0-fold increase in G′, while RENOVITE® NC exhibited a 4.9-fold and 12.0-fold increase, respectively (Fig. S2f).

3.2. NC facilitates long-term localization of BMP2 in vitro and in vivo

The localization of fluorescently labeled BMP2 in CS and NC was investigated using an IVIS. *In vitro* testing demonstrated that, regardless of the concentration of BMP2, approximately 90 % of the fluorescence intensity of BMP2 in CS decayed within 3 h, whereas for BMP2 localized in NC, more than 90 % of the fluorescence intensity was retained over 7 days (Fig. 2A–F). *In vivo* testing showed that more than 80 % of the fluorescence intensity of BMP2 inside CS disappeared within 24 h, regardless of the BMP2 concentration. In contrast, more than 75 % remained within the NC containing 1 μg of BMP2, and more than 65 % remained within the NC containing 2 μg of BMP2 for at least 24 h (Fig. 2J–M). BMP2 in the NC was detectable on day 7, whereas BMP2 in the CS was undetectable on day 3. The fluorescence signal at each time point was normalized to the initial signal, and exponential decay curves were created. The biological half-life of BMP2 *in vivo* was 2.3 h for CS and 40.0 h for NC mixed with 1 μg of BMP2 (Fig. 2I and J) and 1.9 h for CS and 37.3 h for NC mixed with 2 μg of BMP2 (Fig. 2L and M), suggesting that the release profiles were consistent across different BMP2 concentrations. These findings demonstrate that the NC outperformed the CS in facilitating long-term BMP localization.

3.3. NC/BMP2 induces new bone formation with extensive trabecular bone

To examine the bone induction capacity of NC or CS containing BMP2, they were implanted in a mouse subfascial implantation model. Micro-computed tomography (micro-CT) evaluation showed that on day 21, the surrounding cortical shell contour was relatively clear in the CS group; in contrast, the NC group showed extensive high-intensity areas on micro-CT, indicating mineral deposition, although the contour of the

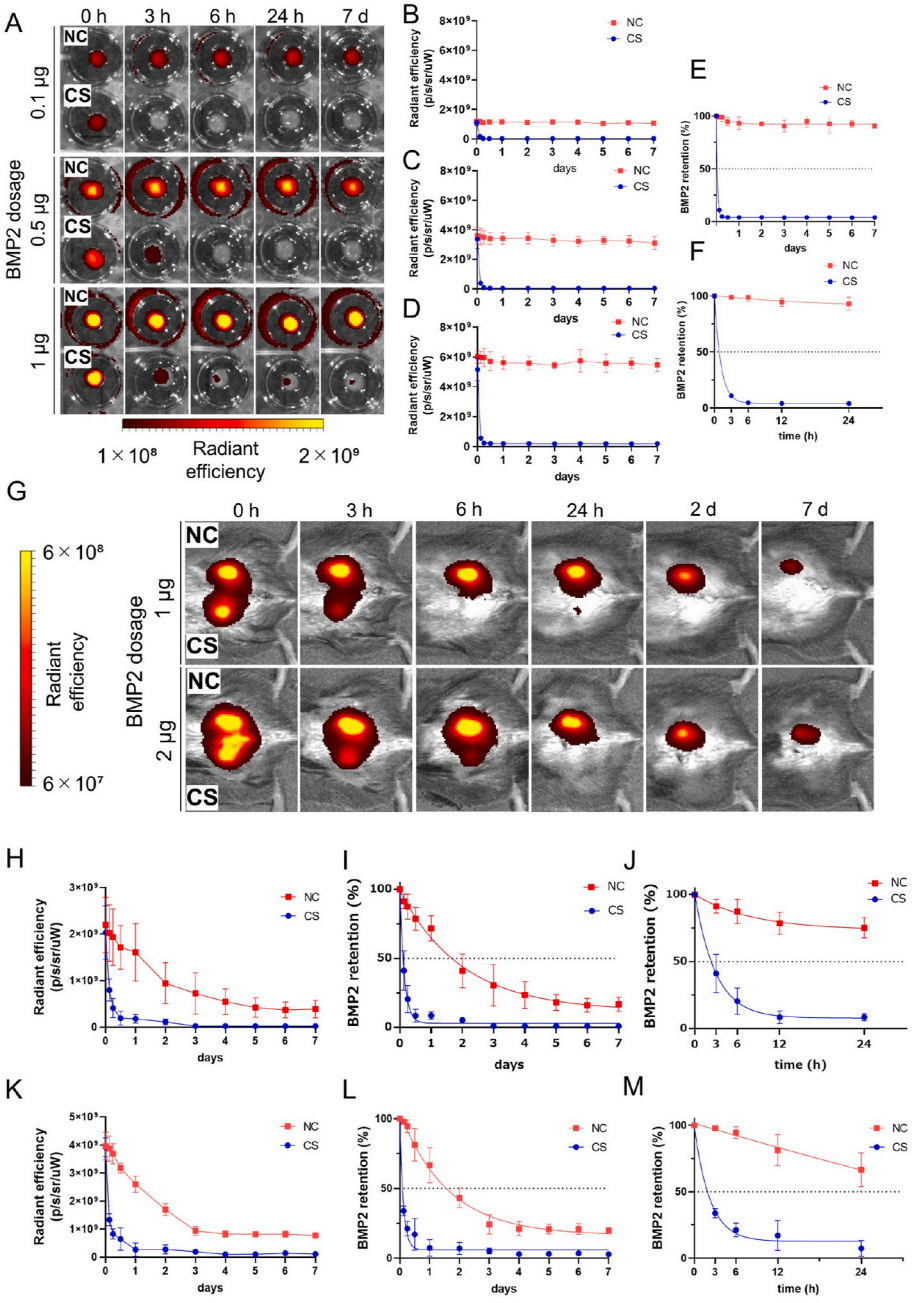

Fig. 2. Retention kinetics of fluorescently labeled BMP2. (A) *In vitro* fluorescence image of CS and NC containing fluorescently labeled 0.1, 0.5, and 1 μg of BMP2 at the bottom of a 24-well plate. *In vitro* radiant efficiency up to 7 days; (B) 0.1 μg of BMP2; (C) 0.5 μg of BMP2; (D) 1 μg of BMP2. Retention kinetics of NC and CS containing 1 μg BMP2 up to 24 h and up to 7 days (E, F). (G) *In vivo* fluorescence image of CS and NC containing fluorescently labeled 1 and 2 μg of BMP2 in a mouse subfascial implantation model. *In vivo* radiant efficiency up to 7 days: (H) 1 μg of BMP2; (K) 2 μg of BMP2. Retention kinetics of NC and CS containing 1 μg of BMP2 up to 24 h and up to 7 days (I, J). Retention kinetics of NC and CS containing 2 μg of BMP2 up to 24 h and up to 7 days (L, M). Data represents the mean ± SD (n = 4 in each group).

cortical shell was indistinct. On day 42, in the NC group, cortical bone was clearly formed in the area surrounding the implant, and, critically, the interior was filled with dense trabecular bone. In contrast, in the CS group, no significant changes were observed in cortical bone formation after day 21, and negligible evidence of trabecular bone structure was detected within the cortical shell (Fig. 3A). The bone mineral density of new bone was significantly higher in the NC group than in the CS group on days 21 and 42 post-implantation ($p < 0.01$, respectively). NC and CS, in the absence of BMP2, did not induce bone formation (Fig. 3B). H&E-stained section images indicated that by day 21, most of the CS had degraded while more gel remained inside the NC, suggesting slower absorption of NC compared to CS (Fig. 3C). Images of H&E-stained sections on day 42 revealed no difference in the thickness of the outer shell of bone surrounding the CS and NC. However, significantly more newly formed bone was observed within NC than CS, consistent with the micro-CT results (Fig. 3D).

3.4. Uniform cartilage formation within NC precedes bone formation

To verify the mechanism by which NC induced high-quality new bone, histological images 7, 10, 14, and 21 days post-implantation were examined. In the CS group, a discrete amount of cartilage tissue stained

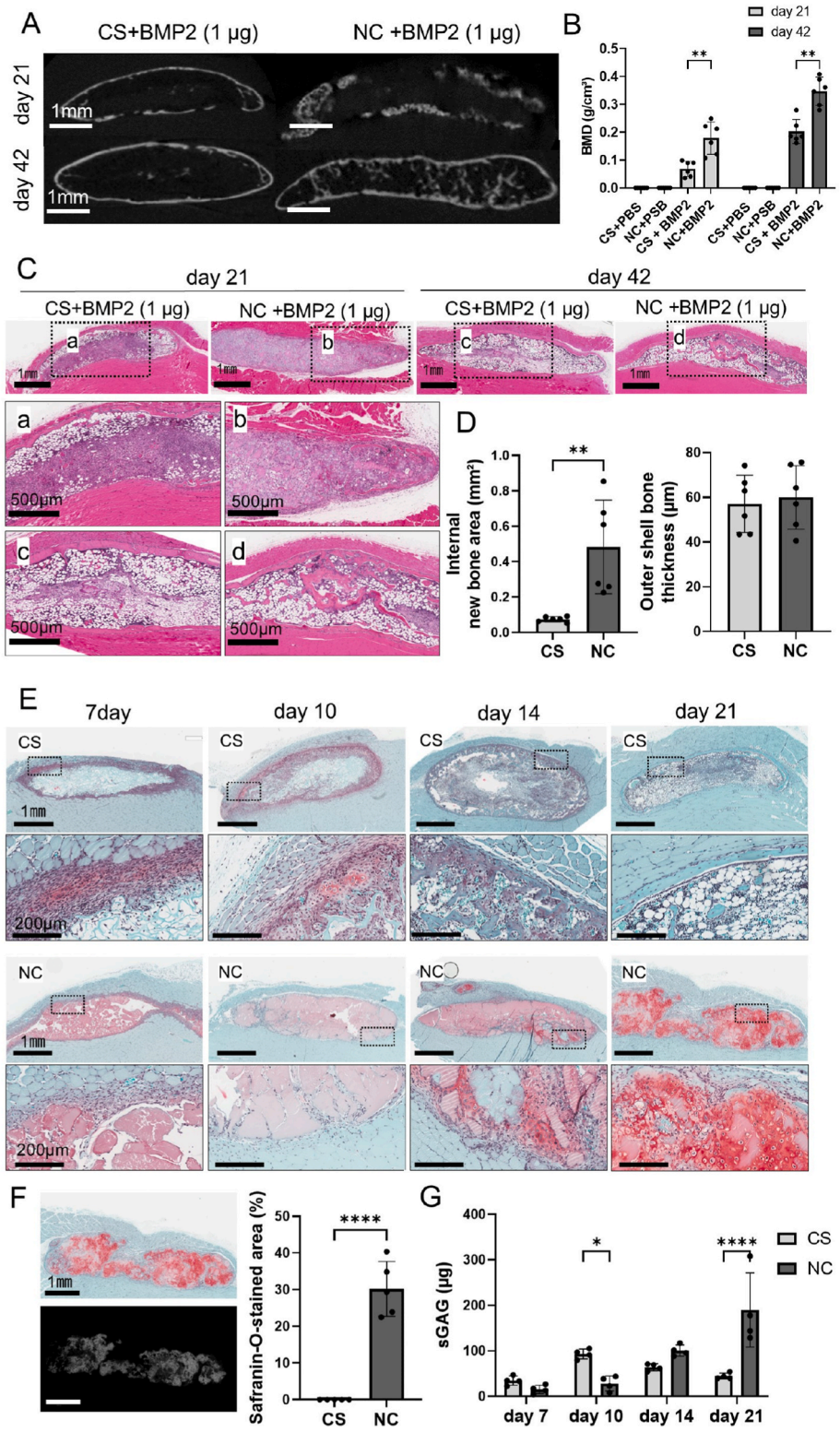

Fig. 3. Evaluation of bone and cartilage formation in the subfascial implantation model. (A) Representative micro-CT images in the CS and in NC groups on day 21 and day 42. Scale bars, 1 mm. (B) Bone mineral density (BMD) of the implanted materials: CS + PBS (n = 6), NC + PBS (n = 6), CS + BMP2 (n = 6), and NC + BMP2 (n = 6). (C) Representative H&E images on day 21 and 42. The NC group showed extensive amounts of bone formation within NC. Scale bars, 1 mm (upper panels), 500 μm (lower panels). (D) Amounts of newly formed bone within the carriers and thickness of the outer cortical shell in the CS and NC groups (n = 6 each). (E) Time-dependent cartilage formation in CS and NC containing 1 μg of BMP2 as evaluated by safranin-O staining. Scale bars, 1 mm (upper panels), 200 μm (lower panels). (F) Quantification of the safranin-O-stained area on day 21 in the CS and NC groups (n = 5 each). Scale bars, 1 mm. (G) Quantitative analysis of sGAG in the CS and NC groups (n = 4 each). Data represent mean ± SD. $*p < 0.05$, $**p < 0.01$, $***p < 0.001$, $****p < 0.0001$ as determined *via* an unpaired *t*-test (D, F) or *via* two-way ANOVA, followed by Bonferroni tests (B, G).

with safranin-O was observed on the outer edge of the CS disc on day 10; this cartilage tissue decreased on day 14 and had completely disappeared by day 21. In the NC group, cartilage tissue was formed from days 14–21 and was widespread inside the NC (Fig. 3E). The CS group showed no safranin-O staining on day 21, whereas approximately 30 % of the implanted sites were stained in the NC group, indicating the substantial presence of a cartilage matrix (Fig. 3F). The areas of bone formation as detected by CT on postoperative day 42 coincided with the areas of cartilage formation in the CS and NC groups, indicating the extensive cartilage formation preceding bone formation in the NC group resulted from endochondral ossification. Quantitative evaluation of the cartilage tissue assessed by measuring sGAG revealed a temporal increase in sGAG up to day 21 in the NC group, whereas, in the CS group, sGAG peaked on day 10 and subsequently decreased on day 21 (Fig. 3G).

3.5. NC does not induce the BMP2 dose-dependent inflammatory response

One of the factors hindering the widespread clinical adoption of BMP2 delivery using a CS carrier is the associated dose-dependent inflammatory response [35–41]. Therefore, we examined the effect of NC on the inflammatory response by implanting CS or NC containing

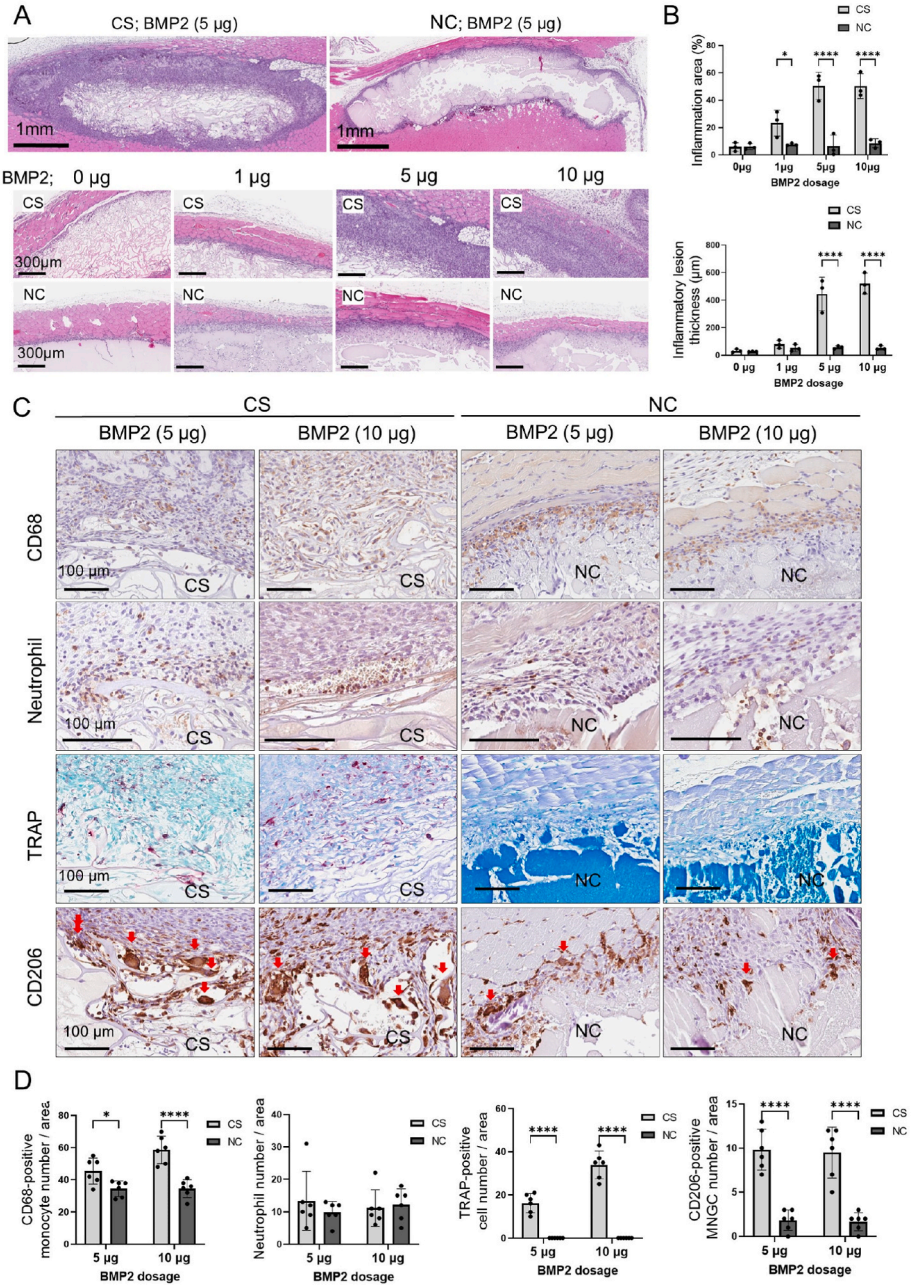

Fig. 4. Effect of NC on the inflammatory response in the subfascial implantation model.
(A) Representative images of H&E-staining sections of subfascial implanted CS and NC containing different concentrations of BMP2 on day 7. BMP2 dose-dependent inflammatory cell infiltration was not observed in the NC group, in contrast to the CS group. Scale bar, upper row: 1 mm, lower row: 300 μm. (B) Quantitative analysis of the area and thickness of the inflammatory lesion in the CS and NC groups (n = 3 each). (C) Immunostaining for CD68, neutrophils, CD206 and TRAP staining of the inflammatory zone around CS and NC containing 5 and 10 μg of BMP2. Scale bars, 100 μm. (D) Quantification of CD68-positive monocytes, neutrophils, TRAP-positive cells, and CD206-positive multinucleated giant cells (MNGCs) (red arrow). Data represent the mean ± SD. *$p < 0.05$, ****$p < 0.0001$, as determined *via* two-way ANOVA, followed by Bonferroni tests.

different amounts of BMP2. In the CS group, the area of inflammatory cell infiltration into the peri-CS tissue expanded in proportion to the BMP2 dose. In contrast, the NC group showed no obvious change in the inflammatory cell infiltration area with increasing BMP2 dose (Fig. 4A and B).

To examine inflammatory cells localized in the inflammatory cell infiltrate layer in more detail, we performed immunostaining for the pan-macrophage marker CD68, MNGC marker CD206, neutrophils, and TRAP. MNGCs are fusions of multiple macrophages caused by foreign bodies or inflammatory reactions; CD206 is a useful marker to distinguish MNGCs from osteoclasts [42]. In the CS group, significant infiltration of CD68-positive monocytes, TRAP-positive cells, and CD206-positive MNGCs was observed compared with the NC group, whereas the number of neutrophils did not differ between the two groups. Notably, the numbers of macrophages and TRAP-positive cells increased in a BMP2 dose-dependent manner. These inflammatory cells were observed in the NC group. However, the numbers of CD68-positive monocytes, TRAP-positive cells, and CD206-positive MNGCs were significantly lower and unaffected by the BMP2 dose (Fig. 4C and D).

Immunostaining for TNF-α showed distinct differences between NC and CS in the appearance of inflammatory cells. In the CS group, the area of inflammatory cell infiltration outside the CS implantation site increased in a BMP2 dose-dependent manner, with little inflammatory cell infiltration into the CS. In contrast, negligible inflammatory cell infiltration was observed around the NC implant site, regardless of the BMP2 concentration; however, BMP2 dose-dependent inflammatory cell infiltration occurred into the NC interior (Fig. 5A and B). Interestingly, the inflammatory cell infiltration area comprised extensive SOX9-positive cells, with particularly strong SOX9 staining within the NC (Fig. 5C and D). This suggests that NC suppresses external inflammation by retaining BMP2, promotes chondrocyte differentiation through prolonged BMP2 localization, induces inflammatory cell infiltration internally, and directly affects bone formation.

3.6. NC/BMP2 enables the formation of a spinal fusion mass filled with trabecular bone

We assessed the effectiveness of NC as a BMP2 carrier using a clinically relevant posterolateral spinal fusion rat model. The bone fusion rate at 6 weeks postoperative at L4/5 posterolateral fusion did not differ between the NC and CS groups, with both groups showing a 100 % fusion rate. However, the quality of the newly formed fusion mass differed significantly between the groups. In the CS group, trabecular bone formation inside the fusion mass was poor, particularly in the high-dose BMP2 (10 μg) group. In the NC group, the interior of the fusion mass was filled with extensive, thick trabecular bone, regardless of the BMP2 dose (Fig. 6A). Micro-CT analysis of the newly formed bone showed that the ratio of bone volume to total volume (BV/TV) and trabecular number (Tb.N) were significantly higher and, as a consequence, trabecular separation (Tb.Sp) was significantly lower in the NC group than in the CS group (Fig. 6C). In the CS group, Tb. Sp was significantly elevated in the high-dose BMP2 (10 μg) group compared with the moderate-dose BMP2 (5 μg) group, whereas in the NC group, there was no significant difference in bone quality. Histological analysis shows that marrow adipose tissue occupied most of the interior of the fusion mass in the CS group, whereas in the NC group, thicker and more extensive trabecular bone and reduced adipose marrow tissue were observed inside the fusion mass (Fig. 7A). The new bone area in the fusion mass was significantly larger in the NC group than in the CS group (Fig. 7B). The adipose tissue area in the fusion mass was significantly larger in the CS group than in the NC group. Additionally, in the CS group, the area of adipose tissue tended to be higher in the high-dose BMP2 (10 μg) group than in the moderate-dose BMP2 (5 μg) group, consistent with the micro-CT analysis (Fig. 7C). These results demonstrate that spinal fusion with extensive, high-quality new bone is achieved when NC is used as a carrier for BMP2.

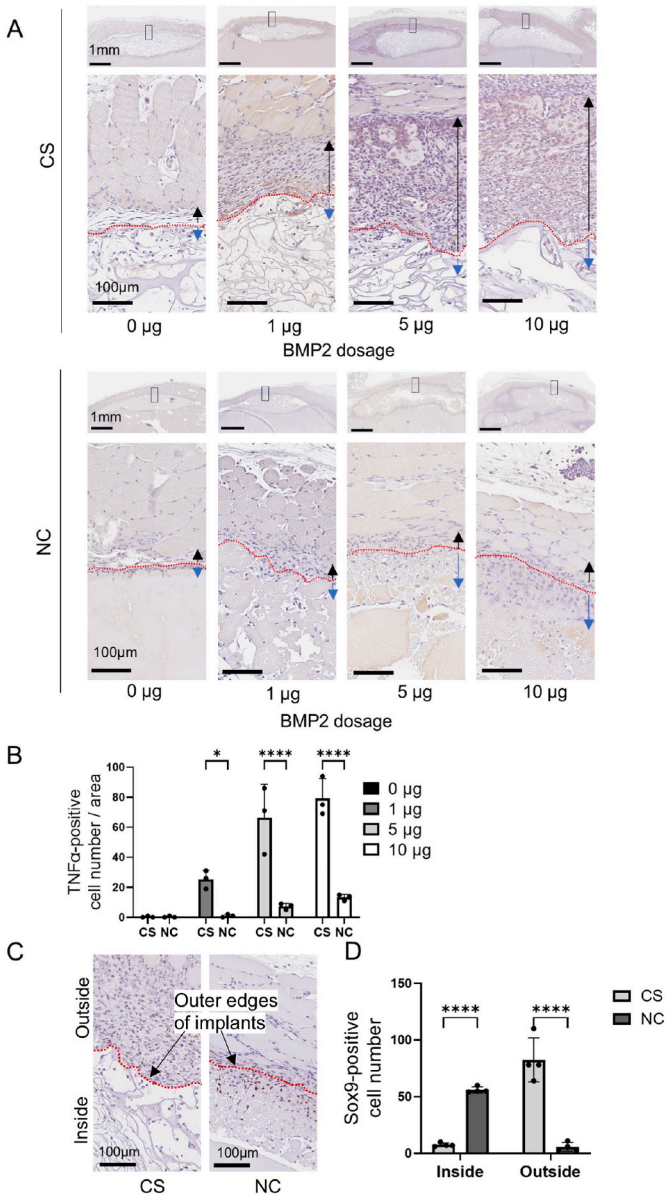

Fig. 5. Assessment of inflammatory responses as assessed by immunostaining. (A) Representative TNF-α immunostaining images for both CS and NC groups. Scale bars, 1 mm (upper panels), 100 μm (lower panels). In the CS group, inflammatory cells were observed infiltrated on the outside (black arrows) rather than inside (blue arrows) of the implant, whereas in the NC group, inflammatory cells could barely be detected outside the NC (black arrow). (B) Quantification of TNF-α-positive cell number (n = 3 each). (C) Representative Sox9 immunostaining images in the inflammatory area around CS and NC containing 5 μg of BMP2. (D) Quantification of SOX9-positive cells inside and outside of the implanted materials (n = 4 each). Scale bars, 100 μm. Data represent the mean ± SD. *$p < 0.05$, ****$p < 0.0001$, as determined *via* two-way ANOVA, followed by Bonferroni tests.

3.7. NC enhances osteoblastic and chondrogenic differentiation

To understand the effects of NC observed *in vivo*, we examined NC effects on osteoblastic and chondrogenic differentiation *in vitro*. When hBMSCs cultured in osteogenic medium were supplemented with NC, no apparent cytotoxicity was observed (Fig. S7a), and a concentration-dependent increase in alkaline phosphatase (ALP) staining (day 7), Alizarin red staining (day 21) (Figs. S3d and f), and the expression of osteogenic genes (*Runx2* and *Col1a1*) occurred on day 7 (Fig. S3e). In MC3T3-E1 osteoblasts, several osteoblast differentiation genes were

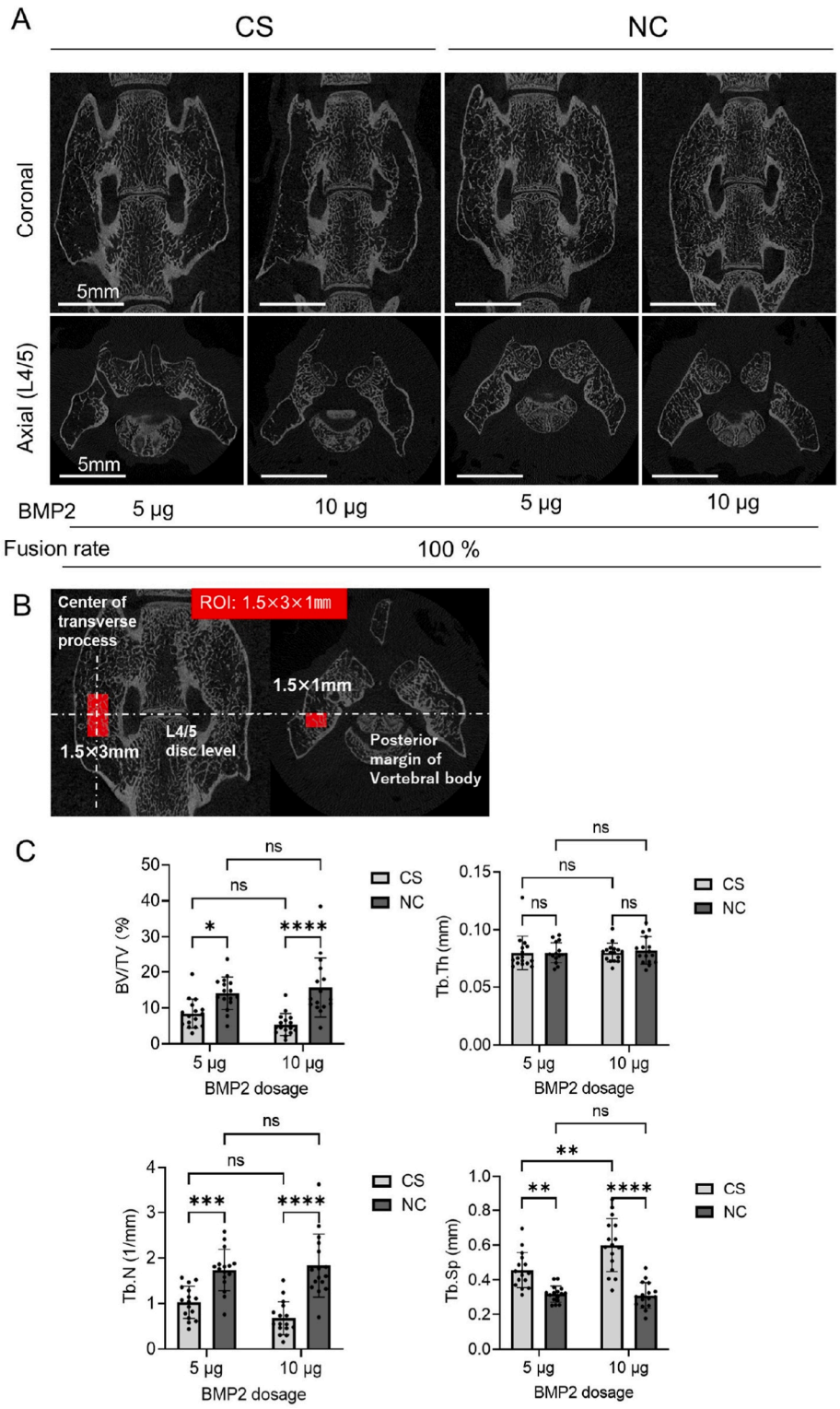

Fig. 6. Micro-CT analysis of spinal fusion model. (A) Illustrative micro-CT images for the CS and NC groups. Scale bars, 5 mm. (B) Placement of a 1.5 × 3 × 1 mm^3 ROI. (C) Microstructural indices of the fusion mass in the CS and NC groups (n = 16 each), including bone volume (BV)/tissue volume (TV), trabecular thickness (Tb.Th), trabecular number (Tb.N), and trabecular separation (Tb.Sp). Data represent the mean ± SD. $^{**}p < 0.01$, $^{***}p < 0.001$, $^{****}p < 0.0001$, as determined *via* two-way ANOVA, followed by Bonferroni tests.

upregulated; however, as the concentration increased, inhibitory effects in MC3T3 were observed. (Figs. S3a, b, c). Furthermore, MC3T3-E1 cells exhibited cytotoxicity at 100 μg/mL, whereas no significant growth inhibition was observed up to 50 μg/mL (Fig. S7b). The concentration-dependent decrease in ALP activity likely resulted from mild toxicity to MC3T3-E1 cells. The differential response to NC concentrations between MC3T3-E1 and hBMSCs underscores the varying balance between effectively stimulating osteoblast differentiation and minimizing cytotoxicity across different cell types, highlighting the necessity for further detailed investigation. The addition of NC to the ATDC5 cell culture

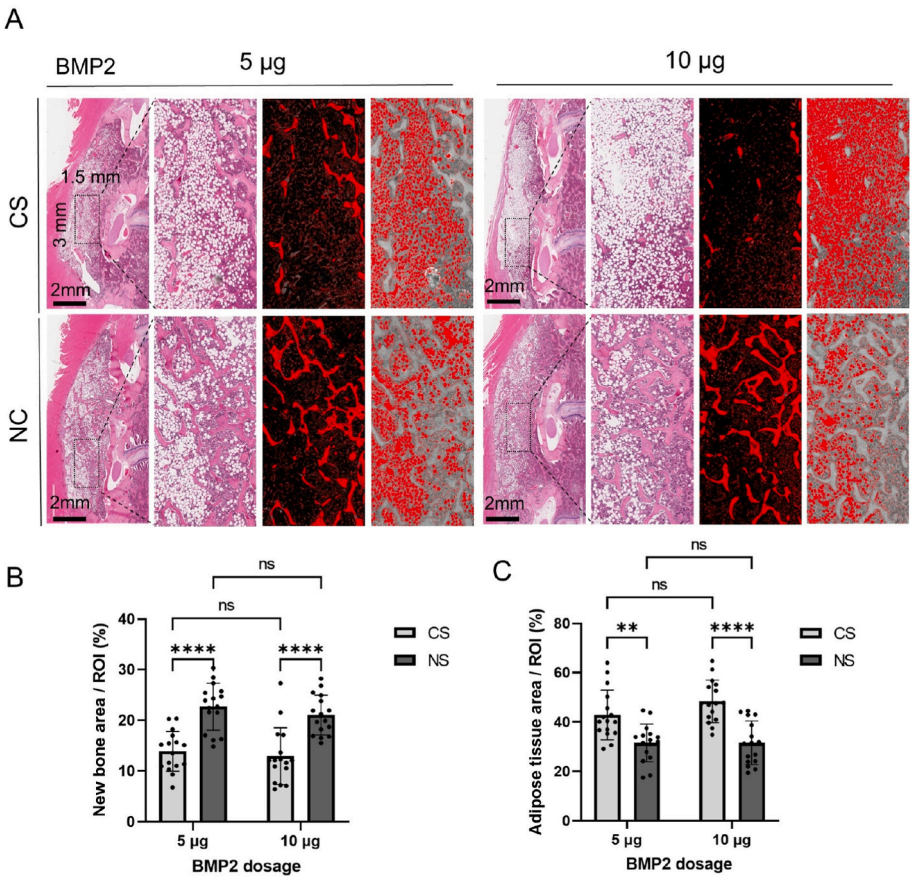

Fig. 7. Histological analysis of spinal fusion model. (A) Comparative assessment of area of new bone formation. A ROI of 1.5 × 3 mm^2 was set inside newly formed fusion mass. New bone areas and adipose tissue areas were color-coded (red) using ImageJ software. Scale bars, 2 mm. (B) Percentage of new bone area within the ROI. (C) Percentage of adipose tissue area within the ROI. Data represents the mean ± SD (n = 16 each). ****$p < 0.0001$, as determined by two-way ANOVA, followed by Bonferroni tests.

medium resulted in no cytotoxicity (Fig. S7c), a concentration-dependent increase in Alcian blue staining on day 7 (Fig. S4a), and the expression of early (*Col2* and *Acan*) and late (*Col10* and *Runx2*) chondrogenic genes (Fig. S4c). The effect of NC on chondrogenic differentiation was confirmed by the enhanced Alcian blue staining of cultured hBMSC micromass cultures (Fig. S4b). Western blot analysis of osteogenic and chondrogenic signaling factors further confirmed the dose-dependent activation of osteogenic and chondrogenic pathways upon the addition of NC (Fig. S4d). Thus, the current findings indicate the potential modulation of osteoblastic and chondrogenic differentiation following NC addition.

3.8. Co-culture with NC containing BMP2 does not affect osteoblast differentiation

Next, we compared CS and NC in a co-culture system to examine the osteogenesis regulation effects in the presence and absence of BMP2 (Fig. S5a). On day 3, ALP staining and activity assessment showed a significant increase in ALP activity in the CS + BMP2 group; this effect persisted through day 7. In contrast, no increase in ALP staining or activity was observed in the NC + BMP2 group, indicating that BMP2 did not diffuse into the surrounding area over the 7 days (Figs. S5b and c). These results are consistent with the *in vitro* release kinetics data (Fig. 2). Furthermore, in the CS- and NC-alone groups, there was no difference compared to the control, indicating that neither CS nor NC degrade *in vitro* or affect the differentiation of distant cells.

3.9. NC suppresses osteoclast differentiation

To investigate the effect of NC on osteoclast differentiation, NC was added to the culture medium of murine primary osteoclast cultures at different concentrations (0.1, 10, and 100 μg/mL). NC significantly suppressed osteoclast formation in a dose-dependent manner (Fig. S6a). Furthermore, the expression of genes related to osteoclastogenesis (*Trap*, *Dcstamp*, *Nfatc1*, and *Ctsk*) was significantly decreased (Fig. S6b). The addition of BMP2 (200 ng/mL) in the culture medium did not significantly alter the results, indicating that even in the presence of BMP2, NC effectively suppressed osteoclast formation.

To determine whether the NC-induced inhibition of osteoclastogenesis was due to cytotoxicity, we evaluated the effect of NC on BMDM viability. Interestingly, after 7 days in culture, no cytotoxic effects were observed at NC concentrations of 10 and 100 μg/mL. Instead, cell proliferation was further promoted (Fig. S7d). This suggests that the inhibitory effect on osteoclast proliferation was not attributable to NC cytotoxicity. To verify the effect of NC on osteoclast differentiation *in vivo*, osteoclast formation in a subfascial implantation model was examined using TRAP staining. In the CS group, extensive TRAP-positive osteoclasts were observed from days 10–14 after implantation. In contrast, in the NC group, few osteoclasts were observed up to day 21 (Figs. S6c and d). These results indicate that NC enhances endochondral bone formation while inhibiting osteoclastic bone resorption.

4. Discussion

The current studies demonstrate NC's capacity to localize BMP2 and to promote extensive bone formation *in vitro* and *in vivo* through

enhanced endochondral bone formation.

NC has very high BMP2 retention properties and a 6-week absorption period without degradation, allowing the BMP2 action to be localized inside the NC for a significant period. Thus, NC retains the osteoinductive ability of BMP2 while suppressing inflammatory responses in the surrounding tissue to a negligible level, preventing ectopic bone formation.

We demonstrated that NC/BMP2-induced new bone formation occurred without a BMP dose-dependent inflammatory response in surrounding tissues, as opposed to the inflammatory response typically observed with collagen carriers currently used in clinical practice.

When used as a carrier for BMP2, NC must withstand pressure from surrounding tissues and localize at the implantation site. Poor localization can lead to NC dispersion into surrounding tissues, causing adverse events such as ectopic ossification. The NC used in this study (RENOVITE®) is a newly developed synthetic hectorite clay for medical applications, which rapidly increases in viscosity *in vivo* and acquires mechanical strength to resist pressure from surrounding tissues. NC exposed to FBS exhibited sufficient mechanical strength to be grasped with forceps, whereas in distilled water, the NC diffused into the surrounding solution (Figs. S2b and c). In the subfascial implantation model, cartilage replaced NC in three weeks and bone in 6 weeks. In addition, in the more clinically relevant spinal fusion model, NC was localized to the implanted sites, allowing for good-quality bone formation with spatial control of bone formation.

The observed efficacy of the NC is likely a consequence of three main features. First, i*n vitro* and *in vivo* BMP2 retention kinetics demonstrate that NC retained BMP2 for significantly longer periods than CS. *In vitro* release kinetics show a negligible change in BMP2 fluorescence intensity over 7 days, demonstrating that the NC slowly released BMP2 with *in vivo* decay, resulting from BMP degradation rather than release. Moreover, CS and NC are inherently biocompatible materials and induce minimal inflammatory responses when implanted *in vivo*. Therefore, we believe that the inflammatory reaction observed around CS containing BMP2 was not caused by CS degradation but by the rapid BMP2 release from CS. Conversely, NC provides a more prolonged retention of BMP2, resulting in reduced inflammation. In addition, the clearance of the clay gel is not mediated by clay particle degradation but by the cellular uptake of intact clay particles and their aggregates [22]. The remodeling rate of the nanoclay gel implant depends on the volume and concentration of the RENOVITE® gel but typically occurs over six weeks (unpublished data).

Uncontrolled burst release of BMP2 has been extensively reported to negatively affect bone formation [43–45]. Excess BMP2 enhances adipocyte differentiation and the formation of adipose tissue instead of trabecular bone within new bone [46,47]. Indeed, BMP-containing NC formed new bone filled with dense trabecular bone, whereas new bone induced by BMP2-impregnated CS formed excess fatty marrow tissue in the subfascial implantation and spinal fusion models (Fig. 3C and 7A). In addition, excessive BMP2 has been widely documented to induce an abnormal bone resorption response [48–50] *via* direct and indirect activation of osteoclasts through increased RANKL expression from amplified osteoblast numbers [51]. In the rat spinal fusion model, within the CS group, Tb. Sp was significantly higher in the high-dose BMP2 (10 μg) group than in the moderate-dose BMP2 (5 μg) group. However, in the NC group, there was no significant difference in bone quality (Fig. 6C). These results indicate that 5 μg of BMP2 is sufficient for bone regeneration of this size using NCs, and conversely, even high doses of BMP2 can be retained inside NCs and do not induce negative effects in the surrounding tissue. The homogeneous environment of the interior of the NC, where bone formation occurs, may have optimized bone formation.

In the subfascial implantation model, CS induced a large number of osteoclasts from day 10 onward, whereas, with NC incorporation, negligible osteoclast formation was observed up to day 21. On day 42, osteoclasts were observed at the perimeter of the new bone in the NC groups; however, few osteoclasts were detected in contrast to those observed early following implantation in the CS group. Furthermore, *in vitro* results showed that NC itself did not exhibit cytotoxicity toward bone marrow-derived macrophages (Fig. S7d) and inhibited osteoclastogenesis (Figs. S6a and b), although the mechanism underlying this inhibition remains to be further verified.

BMP2 produces inflammation-related adverse events in a concentration-dependent manner. Thus, cervical swelling has been reported as a fatal adverse event after off-label use of BMP2 in cervical spine surgery [52,53]. The effect of NC as a BMP2 carrier on the inflammatory response *in vivo* was unexpected. When CS was used as a BMP2 carrier, a dose-dependent inflammatory response was observed in the surrounding tissues, in line with previous findings [28]. In contrast, when NC was used as a BMP2 carrier, negligible inflammation was observed in the surrounding tissues; rather, inflammatory cells were observed to infiltrate the NC in a weak dose-dependent manner. The presence of SOX9-positive cells within the inflammatory area indicated new bone formation in the inflammatory zone, suggesting ectopic bone formation in the CS group (Fig. 5A and B). This observation is significant given the widespread use of BMP2 in the clinic for spinal fusion surgery. Considering the observed BMP2 retention and augmentation of bone formation *in vitro* and *in vivo* and the temporal induction of an osteogenic effect by the NC in the absence of an inflammatory response, the NC carrier offers an innovative technology for temporal and spatially controlled bone formation.

The second feature relates to the chondrogenic and osteogenic effects of NC *in vitro* [21,54]. In addition to the observed biocompatibility and low cytotoxicity [55], NC enhanced osteogenic and chondrogenic differentiation without exogenous bone-inducing factors such as BMPs or dexamethasone. The mechanism underlying the osteogenic and chondrogenic effects of NC is unclear. Although non-toxic nanoclay dissolution degradation products such as Mg^{2+}, $Si(OH)_4$, and Li^+ are often indicated as potential mechanisms, it is likely to involve several different modalities, including i) clay nanoparticle-facilitated transport and exchange of extracellular Ca^{2+} and PO_4^{3-} ions across the cell membrane; ii) the ability of internalized clay nanoparticles to modulate intracellular signaling pathways through clay–protein interactions; iii) clay nanoparticle-mediated receptor interactions or uptake of bioactive molecules [21,56–58]. We demonstrated that NC predominantly promotes osteoblastic and chondrogenic differentiation *via* BMP/Smad signaling. Furthermore, the three-dimensional layered structure of the NC, or the negative charge of its surface, may have contributed to the promotion of chondrogenic differentiation [24,59,60]. Notably, the specific relevance of the *in vitro* effects of clay to the *in vivo* data should be assessed cautiously, as clay gels do not induce bone in the absence of BMP2 when applied *in vivo*.

The third feature is bone regeneration *via* an endochondral ossification process. Bone formation induced by BMP2 typically involves endochondral ossification, although bone formation following BMP implantation *in vivo* can involve intramembranous and endochondral bone formation [61,62]. This difference has been attributed to the heterogeneity of BMP2 concentrations [61,62]. The ability of NC to maintain a constant local BMP2 concentration for a prolonged time may have facilitated controlled endochondral differentiation, leading to high-quality new bone formation. This promotion of bone formation *via* endochondral ossification is particularly useful when the area requiring bone formation is significant, as observed in large bone defects. If a cartilage formation intermediary can be harnessed for filling bone defects, such an approach would be useful in applications requiring bone formation time, including pseudarthrosis and intervertebral spinal fusion, where conditions for bone formation, including blood supply, are poor. In the subfascial implantation model, extensive new bone formation was observed in areas where cartilage formation was observed, indicating that cartilage formation preceded bone formation, contributing to the high-quality new bone formed *via* an endochondral process.

5. Conclusion

In conclusion, NC used as a BMP2 carrier material promotes spatially controlled high-quality new bone formation *via* endochondral ossification without an inflammatory response in the surrounding tissues, in contrast to a CS carrier. These findings indicate the potential of NC as a next-generation BMP2 carrier that reduces the adverse events often associated with current BMP2 clinical use and augurs well for clinical use in a range of orthopedic applications for more active and aging demographics.

CRediT authorship contribution statement

Takuya Furuichi: Writing – original draft, Investigation, Formal analysis, Data curation. **Hiromasa Hirai:** Data curation. **Takayuki Kitahara:** Data curation. **Masayuki Bun:** Data curation. **Masato Ikuta:** Data curation. **Yuichiro Ukon:** Data curation. **Masayuki Furuya:** Investigation, Conceptualization. **Richard O.C. Oreffo:** Writing – review & editing, Conceptualization. **Agnieszka A. Janeczek:** Writing – review & editing, Conceptualization. **Jonathan I. Dawson:** Writing – review & editing, Conceptualization. **Seiji Okada:** Supervision. **Takashi Kaito:** Writing – review & editing, Supervision, Conceptualization.

Ethics approval and consent to participate

All animal experiments were approved by the Animal Experimental Committee of Osaka University Graduate School of Medicine (approval number: 02-027-002) and restrictedly followed ARRIVE guidelines and the National Institutes of Health Guide for the Care and Use of Laboratory Animals.

Funding

This research was financially supported by the JSPS Grant-in-Aid C (20K09479) to TK and research grant (J210701148) by Biosciencepartners Inc.

Declaration of competing interest

The authors declare the following financial interests/personal relationships which may be considered as potential competing interests: Takashi Kaito has received research funding from Japan Society for the Promotion of Science and Biosciencepartners Inc.R.O.C. Oreffo, J. I Dawson and A.A. Janeczek are co-founders and shareholders in a University of Southampton spin out company, Renovos Biologics Limited, with a license to IP indirectly related to the current manuscript.

Acknowledgments

RENOVITE® was kindly provided by Renovos Biologics Limited. rhBMP2 was kindly provided by CGBio Co., Ltd.

Appendix A. Supplementary data

Supplementary data to this article can be found online at https://doi.org/10.1016/j.bioactmat.2024.10.027.

References

[1] T. Kaito, J. Johnson, J. Ellerman, H. Tian, M. Aydogan, M. Chatsrinopkun, S. Ngo, C. Choi, J.C. Wang, Synergistic effect of bone morphogenetic proteins 2 and 7 by ex vivo gene therapy in a rat spinal fusion model, J. Bone Joint Surg. Am. 95 (2013) 1612–1619, https://doi.org/10.2106/JBJS.L.01396.

[2] T. Kaito, A. Myoui, K. Takaoka, N. Saito, M. Nishikawa, N. Tamai, H. Ohgushi, H. Yoshikawa, Potentiation of the activity of bone morphogenetic protein-2 in bone regeneration by a PLA-PEG/hydroxyapatite composite, Biomaterials 26 (2005) 73–79, https://doi.org/10.1016/j.biomaterials.2004.02.010.

[3] J.D. Boerckel, Y.M. Kolambkar, K.M. Dupont, B.A. Uhrig, E.A. Phelps, H.Y. Stevens, A.J. García, R.E. Guldberg, Effects of protein dose and delivery system on BMP-mediated bone regeneration, Biomaterials 32 (2011) 5241–5251, https://doi.org/10.1016/j.biomaterials.2011.03.063.

[4] D. Tang, R.S. Tare, L.Y. Yang, D.F. Williams, K.L. Ou, R.O. Oreffo, Biofabrication of bone tissue: approaches, challenges and translation for bone regeneration, Biomaterials 83 (2016) 363–382, https://doi.org/10.1016/j.biomaterials.2016.01.024.

[5] M.R. Urist, Bone: formation by autoinduction, Science 150 (1965) 893–899, https://doi.org/10.1126/science.150.3698.893.

[6] J.M. Wozney, V. Rosen, A.J. Celeste, L.M. Mitsock, M.J. Whitters, R.W. Kriz, R. M. Hewick, E.A. Wang, Novel regulators of bone formation: molecular clones and activities, Science 242 (1988) 1528–1534, https://doi.org/10.1126/science.3201241.

[7] V.S. Salazar, L.W. Gamer, V. Rosen, BMP signalling in skeletal development, disease and repair, Nat. Rev. Endocrinol. 12 (2016) 203–221, https://doi.org/10.1038/nrendo.2016.12.

[8] J.K. Burkus, E.E. Transfeldt, S.H. Kitchel, R.G. Watkins, R.A. Balderston, Clinical and radiographic outcomes of anterior lumbar interbody fusion using recombinant human bone morphogenetic protein-2, Spine (Phila Pa 1976) 27 (2002) 2396–2408, https://doi.org/10.1097/00007632-200211010-00015.

[9] I.W. Um, J.K. Ku, Y.K. Kim, B.K. Lee, D.H. Leem, Histological review of demineralized dentin matrix as a carrier of rhBMP-2, Tissue Eng., Part B 26 (2020) 284–293, https://doi.org/10.1089/ten.TEB.2019.0291.

[10] D.M. Gibbs, C.R. Black, G. Hulsart-Billstrom, P. Shi, E. Scarpa, R.O. Oreffo, J. I. Dawson, Bone induction at physiological doses of BMP through localization by clay nanoparticle gels, Biomaterials 99 (2016) 16–23, https://doi.org/10.1016/j.biomaterials.2016.05.010.

[11] W. Friess, H. Uludag, S. Foskett, R. Biron, C. Sargeant, Characterization of absorbable collagen sponges as recombinant human bone morphogenetic protein-2 carriers, Int. J. Pharm. 185 (1999) 51–60, https://doi.org/10.1016/s0378-5173(99)00128-3.

[12] W. Friess, H. Uludag, S. Foskett, R. Biron, C. Sargeant, Characterization of absorbable collagen sponges as rhBMP-2 carriers, Int. J. Pharm. 187 (1999) 91–99, https://doi.org/10.1016/s0378-5173(99)00174-x.

[13] W. Friess, H. Uludag, S. Foskett, R. Biron, Bone regeneration with recombinant human bone morphogenetic protein-2 (rhBMP-2) using absorbable collagen sponges (ACS): influence of processing on ACS characteristics and formulation, Pharmaceut. Dev. Technol. 4 (1999) 387–396, https://doi.org/10.1081/pdt-100101374.

[14] D. Tateiwa, S. Nakagawa, H. Tsukazaki, R. Okada, J. Kodama, J. Kushioka, Z. Bal, Y. Ukon, H. Hirai, T. Kaito, A novel BMP-2-loaded hydroxyapatite/beta-tricalcium phosphate microsphere/hydrogel composite for bone regeneration, Sci. Rep. 11 (2021) 16924, https://doi.org/10.1038/s41598-021-96484-4.

[15] J.K. Burkus, S.E. Heim, M.F. Gornet, T.A. Zdeblick, Is INFUSE bone graft superior to autograft bone? An integrated analysis of clinical trials using the LT-CAGE lumbar tapered fusion device, J. Spinal Disord. Tech. 16 (2003) 113–122, https://doi.org/10.1097/00024720-200304000-00001.

[16] R. Oliveira É, L. Nie, D. Podstawczyk, A. Allahbakhsh, J. Ratnayake, D.L. Brasil, A. Shavandi, Advances in growth factor delivery for bone tissue engineering, Int. J. Mol. Sci. 22 (2021) 903, https://doi.org/10.3390/ijms22020903.

[17] D. Tateiwa, T. Kaito, Advances in bone regeneration with growth factors for spinal fusion: a literature review, N. Am. Spine Soc. J. 13 (2023) 100193, https://doi.org/10.1016/j.xnsj.2022.100193.

[18] I. Erezuma, T. Eufrasio-da-Silva, N. Golafshan, K. Deo, Y.K. Mishra, M. Castilho, A. K. Gaharwar, S. Leeuwenburgh, A. Dolatshahi-Pirouz, G. Orive, Nanoclay reinforced biomaterials for mending musculoskeletal tissue disorders, Adv. Healthcare Mater. 10 (2021) e2100217, https://doi.org/10.1002/adhm.202100217.

[19] J.K. Carrow, L.M. Cross, R.W. Reese, M.K. Jaiswal, C.A. Gregory, R. Kaunas, I. Singh, A.K. Gaharwar, Widespread changes in transcriptome profile of human mesenchymal stem cells induced by two-dimensional nanosilicates, Proc. Natl. Acad. Sci. U.S.A. 115 (2018) E3905–E3913, https://doi.org/10.1073/pnas.1716164115.

[20] J.R. Xavier, T. Thakur, P. Desai, M.K. Jaiswal, N. Sears, E. Cosgriff-Hernandez, R. Kaunas, A.K. Gaharwar, Bioactive nanoengineered hydrogels for bone tissue engineering: a growth-factor-free approach, ACS Nano 9 (2015) 3109–3118, https://doi.org/10.1021/nn507488s.

[21] M. Mousa, N.D. Evans, R.O.C. Oreffo, J.I. Dawson, Clay nanoparticles for regenerative medicine and biomaterial design: a review of clay bioactivity, Biomaterials 159 (2018) 204–214, https://doi.org/10.1016/j.biomaterials.2017.12.024.

[22] M. Mousa, Y.H. Kim, N.D. Evans, R.O.C. Oreffo, J.I. Dawson, Tracking cellular uptake, intracellular trafficking and fate of nanoclay particles in human bone marrow stromal cells, Nanoscale 15 (2023) 18457–18472, https://doi.org/10.1039/d3nr02447d.

[23] P. Shi, Y.H. Kim, M. Mousa, R.R. Sanchez, R.O.C. Oreffo, J.I. Dawson, Self-assembling nanoclay diffusion gels for bioactive osteogenic microenvironments, Adv. Healthcare Mater. 7 (2018) e1800331, https://doi.org/10.1002/adhm.201800331.

[24] A.K. Gaharwar, L.M. Cross, C.W. Peak, K. Gold, J.K. Carrow, A. Brokesh, K. A. Singh, 2D nanoclay for biomedical applications: regenerative medicine, therapeutic delivery, and additive manufacturing, Adv. Mater. (Deerfield Beach, Fla.) 31 (2019) e1900332, https://doi.org/10.1002/adma.201900332.

[25] J.I. Dawson, J.M. Kanczler, X.B. Yang, G.S. Attard, R.O. Oreffo, Clay gels for the delivery of regenerative microenvironments, Adv. Mater. 23 (2011) 3304–3308, https://doi.org/10.1002/adma.201100968.
[26] Y.H. Kim, X. Yang, L. Shi, S.A. Lanham, J. Hilborn, R.O.C. Oreffo, D. Ossipov, J. I. Dawson, Bisphosphonate nanoclay edge-site interactions facilitate hydrogel self-assembly and sustained growth factor localization, Nat. Commun. 11 (2020) 1365, https://doi.org/10.1038/s41467-020-15152-9.
[27] M.A. Scott, B. Levi, A. Askarinam, A. Nguyen, T. Rackohn, K. Ting, C. Soo, A. W. James, Brief review of models of ectopic bone formation, Stem Cell. Dev. 21 (2012) 655–667, https://doi.org/10.1089/scd.2011.0517.
[28] D. Tateiwa, T. Kaito, K. Hashimoto, R. Okada, J. Kodama, J. Kushioka, Z. Bal, H. Tsukazaki, S. Nakagawa, Y. Ukon, H. Hirai, H. Tian, I. Alferiev, M. Chorny, S. Otsuru, S. Okada, M. Iwamoto, Selective retinoic acid receptor γ antagonist 7C is a potent enhancer of BMP-induced ectopic endochondral bone formation, Front. Cell Dev. Biol. 10 (2022) 802699, https://doi.org/10.3389/fcell.2022.802699.
[29] J. Li, X. Ren, W. Qiao, H. Shi, T. Yang, S. Ma, B. Li, Y. Zhao, Preparation and bone repair capability of a new plastic bone filler material], Zhongguo Xiu Fu Chong Jian Wai Ke Za Zhi 37 (2023) 302–307.
[30] M.H. Hettiaratchi, L. Krishnan, T. Rouse, C. Chou, T.C. McDevitt, R.E. Guldberg, Heparin-mediated delivery of bone morphogenetic protein-2 improves spatial localization of bone regeneration, Sci. Adv. 6 (2020) eaay1240, https://doi.org/10.1126/sciadv.aay1240.
[31] B.N. Robin, C.D. Chaput, S. Zeitouni, M.D. Rahm, V.A. Zerris, H.W. Sampson, Cytokine-mediated inflammatory reaction following posterior cervical decompression and fusion associated with recombinant human bone morphogenetic protein-2: a case study, Spine 35 (2010) E1350–E1354, https://doi.org/10.1097/BRS.0b013e3181e85756.
[32] K. Shahlaie, K.D. Kim, Occipitocervical fusion using recombinant human bone morphogenetic protein-2: adverse effects due to tissue swelling and seroma, Spine 33 (2008) 2361–2366, https://doi.org/10.1097/BRS.0b013e318183971d.
[33] K. Uchibe, J. Son, C. Larmour, M. Pacifici, M. Enomoto-Iwamoto, M. Iwamoto, Genetic and pharmacological inhibition of retinoic acid receptor γ function promotes endochondral bone formation, J. Orthop. Res. 35 (2017) 1096–1105, https://doi.org/10.1002/jor.23347.
[34] K.J. Livak, T.D. Schmittgen, Analysis of relative gene expression data using real-time quantitative PCR and the 2(-Delta Delta C(T)) method, Methods 25 (2001) 402–408, https://doi.org/10.1006/meth.2001.1262.
[35] N.F. Chen, Z.A. Smith, E. Stiner, S. Armin, H. Sheikh, L.T. Khoo, Symptomatic ectopic bone formation after off-label use of recombinant human bone morphogenetic protein-2 in transforaminal lumbar interbody fusion, J. Neurosurg. Spine 12 (2010) 40–46, https://doi.org/10.3171/2009.4.SPINE0876.
[36] R.K. Shah, V.M. Moncayo, R.D. Smitson, C. Pierre-Jerome, M.R. Terk, Recombinant human bone morphogenetic protein 2-induced heterotopic ossification of the retroperitoneum, psoas muscle, pelvis and abdominal wall following lumbar spinal fusion, Skeletal Radiol. 39 (2010) 501–504, https://doi.org/10.1007/s00256-010-0890-8.
[37] V. Joseph, Y.R. Rampersaud, Heterotopic bone formation with the use of rhBMP2 in posterior minimal access interbody fusion: a CT analysis, Spine (Phila Pa 1976) 32 (2007) 2885–2890, https://doi.org/10.1097/BRS.0b013e31815b7596.
[38] D.A. Wong, A. Kumar, S. Jatana, G. Ghiselli, K. Wong, Neurologic impairment from ectopic bone in the lumbar canal: a potential complication of off-label PLIF/TLIF use of bone morphogenetic protein-2 (BMP-2), Spine J. 8 (2008) 1011–1018, https://doi.org/10.1016/j.spinee.2007.06.014.
[39] R. Vaidya, A. Sethi, S. Bartol, M. Jacobson, C. Coe, J.G. Craig, Complications in the use of rhBMP-2 in PEEK cages for interbody spinal fusions, J. Spinal Disord. Tech. 21 (2008) 557–562, https://doi.org/10.1097/BSD.0b013e31815ea897.
[40] K.U. Lewandrowski, C. Nanson, R. Calderon, Vertebral osteolysis after posterior interbody lumbar fusion with recombinant human bone morphogenetic protein 2: a report of five cases, Spine J. 7 (2007) 609–614, https://doi.org/10.1016/j.spinee.2007.01.011.
[41] T.G. Carter, P.S. Brar, A. Tolas, O.R. Beirne, Off-label use of recombinant human bone morphogenetic protein-2 (rhBMP-2) for reconstruction of mandibular bone defects in humans, J. Oral Maxillofac. Surg. 66 (2008) 1417–1425, https://doi.org/10.1016/j.joms.2008.01.058.
[42] R.J. Miron, H. Zohdi, M. Fujioka-Kobayashi, D.D. Bosshardt, Giant cells around bone biomaterials: osteoclasts or multi-nucleated giant cells? Acta Biomater. 46 (2016) 15–28, https://doi.org/10.1016/j.actbio.2016.09.029.
[43] K.S. Cahill, J.H. Chi, A. Day, E.B. Claus, Prevalence, complications, and hospital charges associated with use of bone-morphogenetic proteins in spinal fusion procedures, JAMA 302 (2009) 58–66, https://doi.org/10.1001/jama.2009.956.
[44] J.N. Zara, R.K. Siu, X. Zhang, J. Shen, R. Ngo, M. Lee, W. Li, M. Chiang, J. Chung, J. Kwak, B.M. Wu, K. Ting, C. Soo, High doses of bone morphogenetic protein 2 induce structurally abnormal bone and inflammation in vivo, Tissue Eng. 17 (2011) 1389–1399, https://doi.org/10.1089/ten.TEA.2010.0555.
[45] A.W. James, G. LaChaud, J. Shen, G. Asatrian, V. Nguyen, X. Zhang, K. Ting, C. Soo, A review of the clinical side effects of bone morphogenetic protein-2, Tissue Eng., Part B 22 (2016) 284–297, https://doi.org/10.1089/ten.TEB.2015.0357.
[46] X. Liao, L. Wu, M. Fu, D. He, Y. Gu, W. Chen, M. Yin, Chondrogenic phenotype differentiation of bone marrow mesenchymal stem cells induced by bone morphogenetic protein 2 under hypoxic microenvironment in vitro], Zhongguo Xiu Fu Chong Jian Wai Ke Za Zhi 26 (2012) 743–748.
[47] I. Takada, Y. Yogiashi, S. Kato, Signaling crosstalk between PPARγ and BMP2 in mesenchymal stem cells, PPAR Res. 2012 (2012) 607141, https://doi.org/10.1155/2012/607141.
[48] J.K. Burkus, H.S. Sandhu, M.F. Gornet, Influence of rhBMP-2 on the healing patterns associated with allograft interbody constructs in comparison with autograft, Spine (Phila Pa 1976) 31 (2006) 775–781, https://doi.org/10.1097/01.brs.0000206357.88287.5a.
[49] J.W. McClellan, D.S. Mulconrey, R.J. Forbes, N. Fullmer, Vertebral bone resorption after transforaminal lumbar interbody fusion with bone morphogenetic protein (rhBMP-2), J. Spinal Disord. Tech. 19 (2006) 483–486, https://doi.org/10.1097/01.bsd.0000211231.83716.4b.
[50] A.W. James, J.N. Zara, X. Zhang, A. Askarinam, R. Goyal, M. Chiang, W. Yuan, L. Chang, M. Corselli, J. Shen, S. Pang, D. Stoker, B. Wu, K. Ting, B. Péault, C. Soo, Perivascular stem cells: a prospectively purified mesenchymal stem cell population for bone tissue engineering, Stem Cells Transl. Med. 1 (2012) 510–519, https://doi.org/10.5966/sctm.2012-0002.
[51] K. Itoh, N. Udagawa, T. Katagiri, S. Iemura, N. Ueno, H. Yasuda, K. Higashio, J. M. Quinn, M.T. Gillespie, T.J. Martin, T. Suda, N. Takahashi, Bone morphogenetic protein 2 stimulates osteoclast differentiation and survival supported by receptor activator of nuclear factor-kappaB ligand, Endocrinology 142 (2001) 3656–3662, https://doi.org/10.1210/endo.142.8.8300.
[52] E.J. Carragee, E.L. Hurwitz, B.K. Weiner, A critical review of recombinant human bone morphogenetic protein-2 trials in spinal surgery: emerging safety concerns and lessons learned, Spine J. 11 (2011) 471–491, https://doi.org/10.1016/j.spinee.2011.04.023.
[53] J.D. Smucker, J.M. Rhee, K. Singh, S.T. Yoon, J.G. Heller, Increased swelling complications associated with off-label usage of rhBMP-2 in the anterior cervical spine, Spine (Phila Pa 1976) 31 (2006) 2813–2819, https://doi.org/10.1097/01.brs.0000245863.52371.c2.
[54] A.K. Gaharwar, S.M. Mihaila, A. Swami, A. Patel, S. Sant, R.L. Reis, A.P. Marques, M.E. Gomes, A. Khademhosseini, Bioactive silicate nanoplatelets for osteogenic differentiation of human mesenchymal stem cells, Adv. Mater. 25 (2013) 3329–3336, https://doi.org/10.1002/adma.202300774.
[55] Q. Yao, K.E. Fuglsby, X. Zheng, H. Sun, Nanoclay-functionalized 3D nanofibrous scaffolds promote bone regeneration, J. Mater. Chem. B 8 (2020) 3842–3851, https://doi.org/10.1039/c9tb02814e.
[56] S. Yoshizawa, A. Brown, A. Barchowsky, C. Sfeir, Magnesium ion stimulation of bone marrow stromal cells enhances osteogenic activity, simulating the effect of magnesium alloy degradation, Acta, Biomater. 10 (2014) 2834–2842, https://doi.org/10.1016/j.actbio.2014.02.002.
[57] P. Han, C. Wu, Y. Xiao, The effect of silicate ions on proliferation, osteogenic differentiation and cell signalling pathways (WNT and SHH) of bone marrow stromal cells, Biomater. Sci. 1 (2013) 379–392, https://doi.org/10.1039/c2bm00108j.
[58] P. Clément-Lacroix, M. Ai, F. Morvan, S. Roman-Roman, B. Vayssière, C. Belleville, K. Estrera, M.L. Warman, R. Baron, G. Rawadi, Lrp5-independent activation of Wnt signaling by lithium chloride increases bone formation and bone mass in mice, Proc. Natl. Acad. Sci. U.S.A. 102 (2005) 17406–17411, https://doi.org/10.1073/pnas.0505259102.
[59] N. Eslahi, M. Abdorahim, A. Simchi, Smart polymeric hydrogels for cartilage tissue engineering: a review on the chemistry and biological functions, Biomacromolecules 17 (2016) 3441–3463, https://doi.org/10.1021/acs.biomac.6b01235.
[60] S.L. Vega, M.Y. Kwon, J.A. Burdick, Recent advances in hydrogels for cartilage tissue engineering, Eur. Cell. Mater. 33 (2017) 59–75, https://doi.org/10.22203/eCM.v033a05.
[61] S. Presciutti, S. Boden, BMP and Beyond: a 25-year historical review of translational spine research at Emory University, Spine Surg. Relat. Res. 2 (2018) 1–10, https://doi.org/10.22603/ssrr.2017-0063.
[62] A. Minamide, M. Kawakami, H. Hashizume, R. Sakata, T. Tamaki, Evaluation of carriers of bone morphogenetic protein for spinal fusion, Spine (Phila Pa 1976) 26 (2001) 933–939, https://doi.org/10.1097/00007632-200104150-00017.